

# Diffusion and velocity correlations of the phase transitions in a system of macroscopic rolling spheres

F. Vega Reyes<sup>1,2</sup> , A. Rodríguez-Rivas<sup>3</sup> , J. F. González-Saavedra<sup>1</sup>  and M. A. López-Castaño<sup>1</sup> 

<sup>1</sup> Departamento de Física, Universidad de Extremadura, 06071, Badajoz, Spain

<sup>2</sup> Instituto de Computación Científica Avanzada (ICCAEx), Universidad de Extremadura, 06071, Badajoz, Spain

<sup>3</sup> Department of Physical, Chemical and Natural Systems, Pablo de Olavide University, 41013, Sevilla, Spain

\* Correspondence: fvega@eaphysics.xyz (F. V. R.)

**Abstract:** We study an air-fluidized granular monolayer, composed of plastic spheres which roll on a metallic grid. The air current is adjusted so that the spheres never loose contact with the grid, so that the dynamics may be regarded as pseudo two-dimensional (or two-dimensional, if the effects of sphere rolling are not taken into account). We find two surprising continuous transitions, both of them displaying two coexisting phases. Moreover, in all cases, we found the coexisting phases display strong energy non-equipartition. In the first transition, at weak fluidization, a glassy phase coexists with a disordered fluid-like phase. In the second transition, a hexagonal crystal coexists with the fluid phase. We analyze, for these two-phase systems, the specific diffusive properties of each phase, as well as the velocity correlations. Surprisingly, we find a glass phase at very low packing fraction and for a wide range of granular temperatures. Both phases are characterized also by a strong anti-correlated velocities upon collision. Thus, the dynamics observed for this quasi two-dimensional system unveils phase transitions with peculiar properties, very different from the predicted behavior in well know theories for their equilibrium counterparts.

**Keywords:** phase transition, diffusion, granular matter

## 1. Introduction

The dynamics of granular matter has been an emerging field for several decades now [1,2]. This is partly due to the many industrial and engineering applications that this kind of materials has [3]; and partly due the fact that granular set-ups can be used as prototype non-equilibrium systems for experiments [4], and also, from a theoretical viewpoint, they allow for the development of the theory of non-equilibrium statistical mechanics [5], fluid mechanics [6] and materials science [7,8]. Moreover, advances on granular dynamics theory have clearly put in evidence that, both at mesoscopic and macroscopic level, the dynamics of granular matter [1,5,9] can present analogous phenomenology to that of molecular matter but is usually present in more complex ways. This is the case, for instance, of phenomena such as stratification [3], diffusion [10–12], segregation [13–16], mixing [3,17], laminar flow [6], hydrodynamic instabilities [18,19], convection [18,20,21], turbulence [22,23], jamming [24,25], memory effects [26,27] and phase transitions [17,28–33], just to name a few. With respect to phase transition, granular matter displays disordered states which can be for instance liquid-like, glassy or hyperuniform states, and ordered structures like nematic phases, hexagonal or cubic crystals. It also shows phases that are exclusive of two-dimensional (2D) systems, like the hexatic phase.

As an example of the higher complexity of granular dynamics, and just out of illustration, the set of steady base flows that can be observed in a plane Fourier/Couette configuration (a fluid confined within two infinite parallel walls) includes those that are present in molecular gases plus new steady flows, that are specific of granular fluids [6]. In particular, the Fourier configuration (two static parallel walls) for a molecular gas yields steady flows with constant heat flux; these constant heat flux states are however possible in a granular gas if the confining parallel walls are moving (Couette configuration) [34]. Moreover, in addition to this complex phenomenology that is also present in simpler forms in molecular matter, there are phenomena in granular matter that do not have an analog in their equilibrium counterparts, like granular nucleation [35], inelastic clustering [36], collapse [4] or velocity correlations that, at low density, clearly violate the molecular chaos assumption [37]. So, granular dynamics can be regarded, from the theoretical point of view, as an extension or generalization of the dynamics of molecular matter [5,38].

In this work, we focus instead in the phase transitions, and order/disorder phenomenology in a monolayer of macroscopic spheres. Spheres are fluidized by turbulent air currents, in such a way that they keep rolling over a horizontal

plane at all times. In this way, the activated dynamics remains as quasi-2D (or pseudo-2D, as preferred). On the other hand, and as it is well known, an equilibrium fluid in two-dimensions crystallizes to a hexagonal phase via a continuous transition that is mediated by a phase that is specific of two dimensions (the hexatic phase). This process is well described by the KTHNY scenario (from their main authors Kösterlitz, Thouless, Halperin, Nelson, Young; see their independent works [39–42]). The hexatic phase appears exclusively in 2D and is characterized by having quasi-long-ranged orientational correlations (with power-law slow decay) and short-ranged translational correlations (with exponential decay). By contrast, the hexagonal crystal shows quasi-long-ranged translational order. Thus, as the crystal melts, long translational order is lost, and correlations undergo a complete transformation process towards complete disorder, which characterizes the liquid phase [43].

This liquid-hexatic-crystal scenario has been observed in non-equilibrium systems as well, although with (eventually) important variations. For instance, the hexatic phase has been detected in a monolayer of vertically vibrated macroscopic spheres [44,45]. More specifically, in the work by Olafsen & Urbach [44], the phenomenology for the quasi-2D non-equilibrium system appears to be rather similar to that described for equilibrium systems that are strictly two-dimensional. To the point that virtually no difference with respect to the equilibrium theory was detected. In effect, a first transition was found, where the crystal melts to the intermediate hexatic phase described by the KTHNY scenario, by means of a process of unbinding of dislocation pairs in the hexagonal lattice. A second transition consecutively occurs, where the hexatic phase decays to a liquid-like phase with complete disorder, through a process of gradual unbinding of disclinations. In this way, the crystal melting process occurs as a double continuous transition, without a coexistence with the liquid phase ever taking place, unlike in three-dimensional matter. In the work by Olafsen & Urbach [44], however, experiments were performed only with stainless steel spheres, which are nearly elastic (see the work by Louge and collaborators [46], accompanied with the comprehensive data table [47], where the coefficients of restitution for steel and other metals are given). In fact, the corresponding velocity distribution shows little to no deviations off the Maxwellian distribution [48,49], meaning that the system is not far from equilibrium [50,51]. In this way, one can say that for the phase behavior might be expected not to differ much from that of a truly equilibrium system. In this sense, further experiments, performed by Komatsu & Tanaka [45], with the same monolayer configuration found an intriguing disappearance of the KTHNY scenario for rubber spheres, which are more inelastic than steel spheres [47]. They observed an abrupt change from continuous to discontinuous melting. In fact, the melting transition for very inelastic spheres was found exhibit phase coexistence between the crystal and the liquid, without the hexatic phase ever showing up in the process; i.e., the KTHNY scenario disappears completely at high inelasticity. (In fact a previous result for brass spheres, also more inelastic than stainless steel [47], in a two-layer system, already proved that increasing the degree of inelasticity can alter importantly the phase behavior of the granular layer [30].)

Furthermore, the 2D phase behavior in active matter seems to be even more complex than in granular matter. In fact, a complex mélange between the KTHNY scenario with the motility-induced phase separation (that is characteristic of active matter [52]) can be observed for wide ranges of particle density and at strong particle activity [53]. In summary, according to strong experimental and computational evidence, the KTHNY scenario is only one of the possible realizations of the phase behavior in 2D or nearly 2D non-equilibrium systems, and frequently appears mixed with other transitions. Moreover, these alternative scenarios in equilibrium systems seem to be depend upon the type of interaction between the particulate system constituents [43]. In this sense, the KTHNY scenario is not the only possible phase behavior in two-dimensional systems was in fact also predicted for equilibrium systems as well. In effect, first order transitions in 2D equilibrium systems seem to be viable, according to theoretical analysis and Monte Carlo simulations, if dislocation and disclination unbinding are concurrent [43]. Moreover, this concurrence appears to depend upon the features of the interactions between the particles of the system. Therefore, particle interactions seem to play an important role in the phase behavior in 2D.

The present work, which deals with a system of air-fluidized ping-pong balls, is motivated by the previous discussion on the phase behavior in 2D particulate systems. In this sense, previous experimental observation puts in evidence the existence of long-ranged repulsive interactions between the air-fluidized particles [54]. This interaction, whose origin lies in the usual hydrodynamic interactions due to the presence of the interstitial fluid [55] (air in this case), is absent in the case of the vibrated system. Moreover, this repulsion does not prevent particle direct encounters (collisions) [56,57]. Thus, due to the combined action of inelastic collisions plus repulsive potential between particles, a different phase behavior could be expected, according to the theoretical discussion above for their equilibrium analogs. Analysis of

eventual departures from the KTHNY scenario when long-ranged hydrodynamic interactions would be relevant for a more complete understanding of the phase behavior in two-dimensional systems. Although this experimental configuration has been studied in a number of previous works [54,57–60], they have focused on different features of the complex dynamics that this type of system exhibits, and no detailed analysis has been carried out on the phase behavior, except for some previous work where a generic description has been provided [57,60].

For this reason, we focus in this work on the specific features of the observed phases and the transitions between them. As we will see, several discontinuous phase transitions can clearly be detected as air upflow intensity is increased, giving rise to states with either a single phase or two coexisting phases. We will study the granular temperature field (here defined as  $T = (1/2m\langle v^2 \rangle)$ , where  $\langle v^2 \rangle$  the square of particle velocity spatially averaged over all steady states), as well as the structure (particle density, pair correlation function) and dynamical properties (diffusion and velocity autocorrelations) of each of the observed phases. The combined analysis of these magnitudes allows us for identifying the the following phases: arrest phase, glass, liquid and hexagonal crystal. In particular, we show that the glass and the crystal phases are clearly subdiffusive. Surprisingly, the liquid phase can display either normal diffusion or weakly subdiffusive (or superdiffusive) behavior. As we will see, these transitions in the diffusive behavior of the system occur in a discontinuous way. Furthermore, in the glassy phase, particle velocities are strongly anticorrelated at early times, whereas the crystal anticorrelations are weak. We also found strong energy non-equipartition in all cases of two coexisting phases.

The paper is structured as follows: Section 2 is devoted to the description of the experimental set-up and methods, and also to a qualitative description of the observed phase behavior. In Section 3, the results for particle diffusion and velocity correlations of each of the observed phases are analyzed separately and in detail. Finally, in Section 4 the results and final conclusions are discussed.

## 2. Description of the experiments

### 2.1. Setup

The experimental configuration we use in this work was designed in our lab. It consists of an air-table set-up [61]. In our case, it is composed by two essential parts: a) the driving unit, that produces a stable quasi-laminar air upflow, consisting of a high power fan (SODECA HCT-71-6T) coupled to a system of short tunnel winds; and b) the arena, which consists of a flat metallic plate with a hexagonal lattice of perforated circular holes (of 3 mm diameter) is surrounded by circular walls (PLA plastic) of 4.5 cm height. The metallic plate is carefully levelled to be horizontal (so that gravity does not enter into the dynamics if restrained within the plate). Both parts are connected by a pair of perpendicular channels that conduct the air released from the fan upwards to the metallic grid. See Figure 1 for a schematic representation of this configuration. A set of spherical particles (ping pong balls, made of ABS plastic with mass density  $0.08 \text{ g cm}^{-3}$ ) are disposed over the metallic grid. The spherical particles are all identical, having a diameter of  $\sigma = 4 \text{ cm}$  and a mass density  $\rho = 0.08 \text{ g cm}^{-3}$  (ABS plastic material). The metallic grid has a square-shaped ( $80 \times 80 \text{ cm}^2$ ). A (circle-shaped) plastic wall is put inside it, centered, so that the particles are enclosed within this circular region of radius  $R = 36.25 \text{ cm}$ .

In the between of the conducting channels there is a foam that homogenizes the upflow. This foam helps the upflow to reach under quasi-laminar conditions, when impinges from below the set of spherical particles. This ping-pong ball on air table configuration is inspired in a previous work by Ohja et al., where the solution to the equation of movement of a Brownian particle (consisting on a ping-pong ball in an air table) was found and compared to their experimental results [12]. Fan power is carefully adjusted so that the particles never loose physical contact with the plate and so they keep rolling over the grid, much in the same way of the aforementioned and other previous works [12,56–58,60].

Within the appropriate ranges of fan power, air upflow past the spheres produces turbulent vortexes [12,57,62,63] that yield stochastic horizontal movement to the spheres and thus the particle dynamics (if sphere rolling is excluded) is strictly two-dimensional. For a dimensional analysis with similar particles, please refer to the methods section in [12] and/or supplementary material file in [57]. As fan power is increased, the system passes through a series of different physical configurations which are accessed through phase transitions. We have observed phase coexistence during these transitions, for experiments in a range of values of particle density. We characterize particle density by means of the packing fraction, that here is defined as  $\phi \equiv N\sigma^2/(4R^2)$ , where  $N$  is the number of particles present in the system. For this set of experiments we used  $40 \leq N \leq 252$ , which roughly corresponds to packing fractions  $0.12 < \phi < 0.76$ . All curves presented in the manuscript result from averaging over all of the present particles in each experiment.

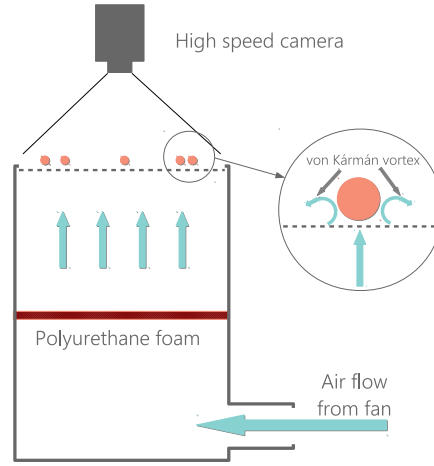


**Figure 1.** Sketch of the experimental set up.

We perform each experiment by setting the fan on to a constant power. Once a stationary state is achieved, we record the particles dynamics from above by means of a high-speed camera (Phantom VEO 410L) at 250 fps. We double check afterwards that the registered interval of the experiment is in effect under steady state conditions by plotting vs. time the relevant space-averaged magnitudes (e.g., average kinetic energy). In any case, it is rather straightforward to ensure steady state conditions by waiting for a time interval equivalent to several collisions per particle [64]. Since the recorded stationary section of the experiment that is recorded is always 100 s long, a large set of steady state statistical replica corresponding to recorded frames available to process ( $\approx 2 \times 10^4$ ). In this way we can achieve statistical accuracy of our data. Data sets are obtained by processing experiments movies with a particle tracking code that we developed specifically for this configuration. This code is composed by a series of OpenCV [65] and TrackPy [66] functions, which allow to obtain all particle positions over the acquired images and tag each particle so that it will be tracked through the entire movie. An exact copy of the particle tracking code (in python language) is freely accessible [67].

## 2.2. Phase behavior

Figure 2 presents a series of movie snapshots displaying the different phase states that we have detected in our experiments, for two different packing fraction values ( $\phi = 0.18$  for the first row,  $\phi = 0.55$  for the second row). For each packing fraction, snapshots are placed in ascending order of fan power. For  $\phi = 0.18$  and the lowest fan power, a subset of particles is still static, since the turbulent vortexes intensity is not strong enough so as to overcome static friction. We denote this static phase as *arrest* phase, due to its static nature. It corresponds to the upper right corner in Figure 2 (a). Interestingly, the arrest phase has been detected before in analogous configurations [4] and is known to develop a quasi-static ordered state that has been denoted as *collapse* phase. If current intensity is high enough, however, a subset of the spheres can activate its thermal-like movement (that, as we discussed, is due to the turbulent vortexes generated by the upflow past the spheres). Their movement is initially limited, so that we can observe caging effects for these particles (bottom left section in Figure 2 a). Thus, we have detected coexistence between the arrest phase and a glassy phase for the caged moving particles (Figure 2 a). The arrest phase eventually disappears as particles gradually activate, then giving rise to a pure glass phase and afterwards (at stronger upflow intensity) to glass-liquid phase coexistence (for this coexistence, see Figure 2 b, with the glass phase occupying the lower density region in the upper right corner of the snapshot). At higher density ( $\phi = 0.55$ , we observe consecutively: liquid phase (Figure 2 c), liquid-crystal coexistence (the crystal is hexagonal, see the developing hexagonal structure, with some defects, in bottom right corner in Figure 2 d), and crystal-liquid phase (Figure 2 e). At this point, if fan power is still increased, a gradual shrink of the hexagonal crystal (which *melts*). The crystal completely disappears above a threshold value of air current intensity. At this point, only the liquid remains (again). This last stage is not represented since they look much like the snapshots in Figure 2 (c),(d). In any case, grasping the phase configuration out of these snapshots is not straightforward and for this reason we analyze in more detail the particle trajectory structure in the next section.

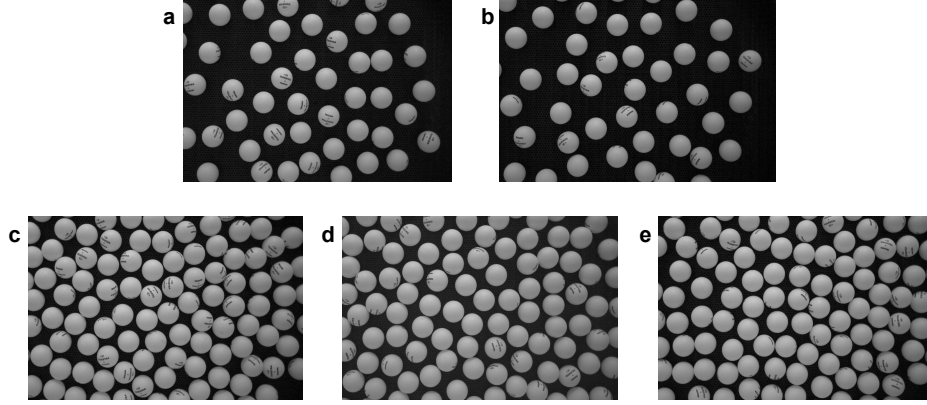


**Figure 2.** Snapshots of the different phase configurations observed in experiments. Packing fraction is  $\phi = 0.18$  for (a)-(b) and  $\phi = 0.55$  for (c)-(e). Granular temperatures are, in order:  $T/m = [0.16, 0.74, 0.38, 0.47, 0.70] \sigma^2 s^{-2}$  for the configurations (same order): glass-arrest phase, glass-liquid, liquid, crystal, crystal-liquid.

### 3. Results

#### 3.1. Trajectories and granular temperature field

In order to analyze in more detail the dynamic properties (except for the static arrest phase), we analyze separately, for each phase, the trajectory shape, temperature field, and the properties of diffusion and velocity autocorrelations. We define the temperature field as  $T(x, y) = (1/2) \langle v^2 \rangle_{xy}$ , where  $\langle v^2 \rangle_{xy}$  stands for the square of particle velocity ( $v$ ) averaged, at a given point  $(x, y)$  of the system, through all measured steady states. In this work, we use the concept of granular temperature (or simply, temperature) in the same sense as first defined by Kanatani [68].

Let us comment now on the phase behavior and the transitions we detected. In the first transition, at low granular temperature, a glass is observed in coexistence with an arrest phase. By arrest phase we refer to particles that, at very low energy input, lie still due to friction [4,32]. In the second phase transitions, glass decays to a liquid-like phase, coexisting with it as it shrinks. At even higher temperatures, a hexagonal crystallite develops, in which we can observe in certain ranges of driving intensity a coexistence between a liquid and a hexagonal crystal [57]. Moreover, We have detected strong energy non-equipartition occurs between the coexisting phases.



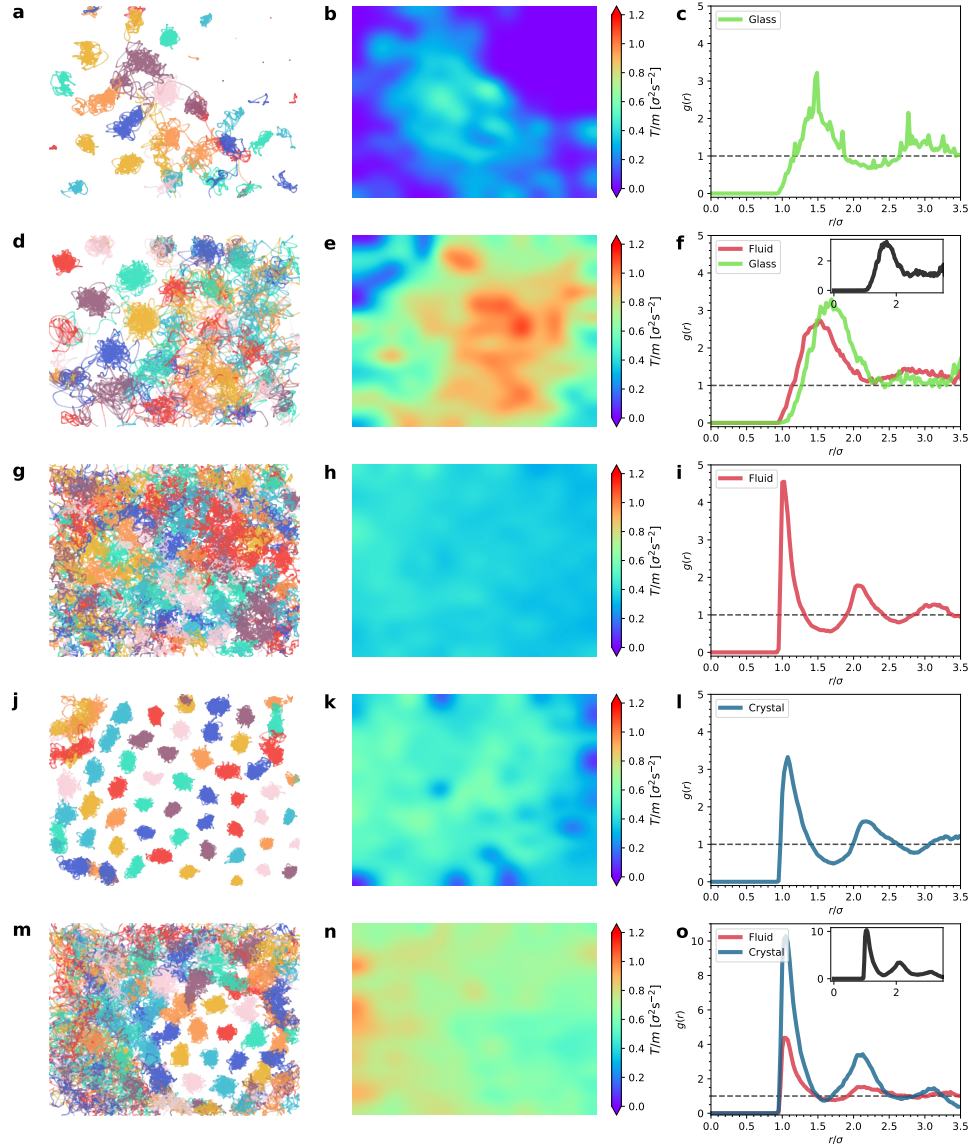


**Figure 3.** Phase behavior of our system, in a central region of interest. Left column represents particle trajectories; right column shows the corresponding granular temperature 2D fields ( $T$ ). Packing fraction is  $\phi = 0.18$  for (a)–(f) and  $\phi = 0.55$  for (g)–(o). Meanwhile, granular temperatures for each pair of panels are, respectively:  $T/m = [0.16, 0.74, 0.38, 0.47, 0.70] \sigma^2 s^{-2}$ . In (a)–(c) we can see phase coexistence between a glassy phase and the arrest phase at low density. In (d)–(f), low density but higher  $T$ , there is glass and liquid phase coexistence. (g)–(i) shows that the system is completely disordered (there is only a liquid phase), state that can be observed at intermediate temperatures for all densities. At higher densities, if the liquid is further heated (air upflow is increased), a cooler crystallite develops in coexistence with the liquid; the crystal grows as  $T$  is increased, eventually occupying the entire system, as in (j)–(l). At stronger driving, the liquid tends to disappear and the crystal occupies the whole system, as seen in (m)–(o).

These results are illustrated in Figure 3. This figure shows, for a representative set of experiments, particle trajectories in the left column, 2D color maps of the granular temperature  $T(x, y)$  in the middle column and pair correlation function  $g(r)$  in the right column. The experiments shown in Figure 3 correspond to two different densities (low, with  $\phi = 0.18$  and high, with  $\phi = 0.55$ ), with each subset in ascending order of upflow current intensity. In it, we can see the phases that consecutively appear as more energy is input into the system. Figure 3 (a) shows two qualitatively different types of arrangements of particle trajectories phases: a disordered lattice of caged particle trajectories (caged in the sense that moving particles remain close to a disordered set of fixed points), and a disordered lattice of static particles (arrest phase).

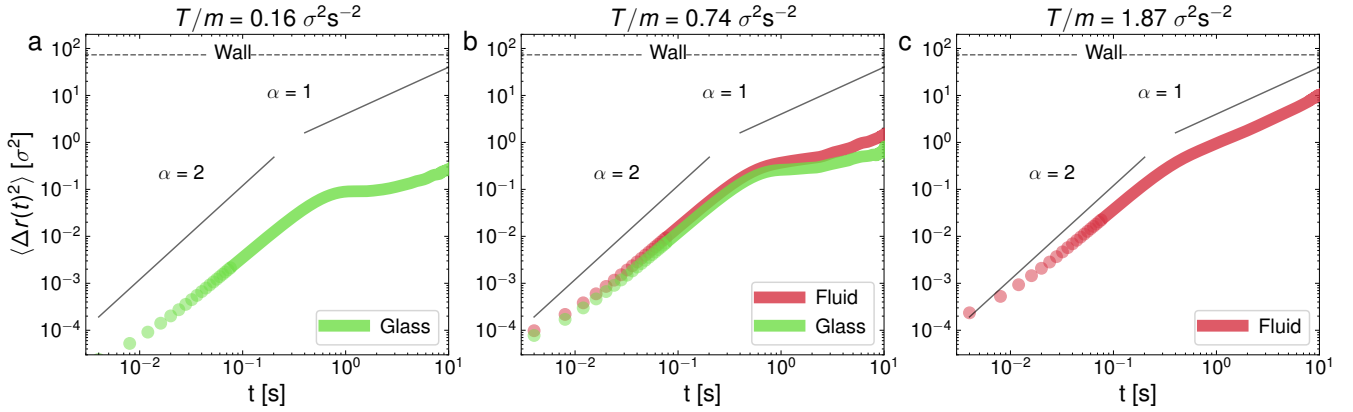


**Figure 4.** Log-Log representation of the mean squared displacement for three representative experiments of  $\phi = 0.18$ , the central panel corresponds to the case presented in Figure 3(c)-(d).

In effect, the former set of trajectories can be identified as a glassy phase since, although particles undergo continuous stochastic movement, caging effects are predominant [69,70] and a disordered but permanent particle trajectory structure (lattice) can be observed. To our knowledge, it is not very common to find glass transitions at such low densities. With respect to the latter, it is apparent that particles remain static during the complete 100 s experiment. From this qualitative difference between these two phases a strong energy non-equipartition emerges. In effect, as we can see in Figure 3 (b), the region corresponding to the arrest phase has vanishing granular temperature  $T$  whereas for the glassy phase  $T$  is clearly non-null. Note that, contrary to what has been observed in thin layers, we have not detected a static phase that yields a hexagonally ordered collapse phase, as in a vertically vibrated monolayer of spheres [4]. This peculiar arrest phase, that is present also in a vibrated granular monolayer [32], disappears here gradually as the upflow current is increased, to a point where we can observe two-phase coexistence between glass-like and liquid-like phases, as in Figure 3 (c), where the liquid phase is observed in the region where all trajectories mix and cross each other during the experiment, in contrast with the disordered pattern of localized trajectories that is visible in the upper left corner. As usual [69], the corresponding  $g(r)$  curves for the glass phases (see green curves in Figure 3 c,f) do not help to distinguish the glass phase from the liquid phase. We will have to resort to the peculiar dynamic properties of the glass for that matter (mean squared displacement and velocity autocorrelations). As we can see in Figure 3 (e), energy non-equipartition is strong here again, with the glass phase being noticeably cooler. At higher density (packing fraction  $\phi = 0.55$ ), we observe, consecutively, a monophasic liquid-like system (Figure 3 f-h); a hexagonal crystal phase (Figure 3 i-k); and a two-phase system, with a liquid coexisting with a hexagonal lattice (Figure 3 i-j). With respect to the corresponding behavior of their pair correlation function,  $g(r)$ , the curves for the liquid and the crystal are noticeably different, with the curves for the crystal having stronger secondary peaks, as usual [44]. With respect to  $T(x, y)$ , notice also that non-equipartition is also present in the case of the liquid-crystal two phase system, with the crystal colder than the liquid (Figure 3 h).

Overall, the fact that non-equipartition is noticeably present in all two-phase system configuration denotes that each phase has its own peculiar dynamics. In particular, this can be an indication that the diffusion process in each phase might have different scales and behavior [71]. In this sense, note the structure of Brownian trajectories in each phase is very different, as trajectories in the left column of Figure 3 show. For this reason, by identifying first which trajectories belong to each phase in all experiments (with the aid of the average coordination number for each particle, as extracted from the corresponding Voronoi tessellations [57]), we have computed the diffusion coefficient for each phase. This allows us for tracking the mean squared displacement (MSD) for each phase independently. Figures 4, 5 show the evolution of the ensemble mean squared displacements, that in 2D can be defined as

$$\langle \Delta r(t)^2 \rangle \equiv \langle \Delta x(t)^2 + \Delta y(t)^2 \rangle, \quad (1)$$

where  $\Delta x(t)^2 \equiv (1/\mathcal{N}(t)) \sum_{\{t_0\}} [x(t+t_0) - x(t_0)]^2$  (and analogously for  $\Delta y(t)^2$ ). For each lag time, and under steady state conditions, the squared displacements  $\Delta x(t)^2, \Delta y(t)^2$  can be obtained from averages over the  $\mathcal{N}(t)$  available initial times  $t_0$  (basically,  $\mathcal{N} = N \times N_{\text{st,frames}}$  where  $N_{\text{st,frames}}$  is the number of images taken under steady state conditions, in our case,

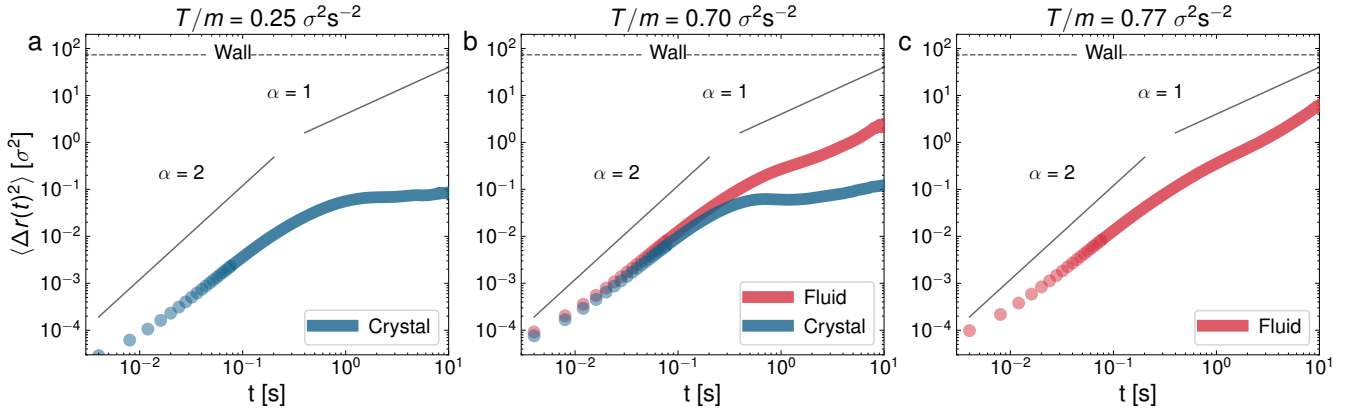


**Figure 5.** Log-Log representation of the mean squared displacement for three representative experiments of  $\phi = 0.55$ . The central panel corresponds to the case presented in Figure 3(i)–(j).

$N_{\text{st,frames}} \approx 25000$ ). The diffusion coefficient can be obtained from the MSD, since most commonly the following relation is fulfilled [57,71]

$$\langle \Delta r(t)^2 \rangle = (4D)t^\alpha, \quad (2)$$

where  $\alpha$  is a constant usually called diffusive exponent. (When Equation 2 is not fulfilled, diffusion is said to be anomalous [71]). Trivially from (2), the diffusive exponent  $\alpha$  corresponds to the slope of the diffusive part, in a Log-Log representation, of the MSD vs. lag time, as in the curves displayed in Figures 4, 5. By diffusive part we mean, as usual, the part of the MSD vs. time curve that is after the ballistic regime, which should always have  $\alpha = 2$  [71]. As a guide to the eye, the ballistic ( $\alpha = 2$ ) and normal diffusion ( $\alpha = 1$ ) diffusion values were indicated inside each panel in Figures 4, 5. We have found however that the slope in the diffusive part of the MSD curves is not constant in some cases, and it may be said that diffusion is in these cases anomalous, which is in agreement with the experimental observations a previous analysis [60]. Thus, the computed diffusive exponents  $\alpha$  for these cases, and the corresponding slope (and thus, diffusion coefficient) from Equation 2 represent an averaged value.

In Figure 4, at low packing fraction ( $\phi = 0.18$ ) we can see the MSD for the following cases: observed; glass (a), glass-liquid (b), liquid (c); whereas in Figure 5 we can see the cases: only crystal (a), crystal-liquid (b) and only liquid (c). It is very apparent that the behavior of the MSD for each phase is very different. In particular, the monophasic glassy configuration (Figure 4 a) presents a MSD with a local maximum at the end of the ballistic regime, after which it presents a characteristic curvature in the diffusive part of the curve, which is besides strongly subdiffusive. The MSD behaviour of the glass-like phase is thus characterized by a short plateau in the MSD followed by an increase (when particles escape the current "caging" area and move to a new location). At higher  $T$ , in Figure 4 (b), we can see the glass-liquid coexistence. In this case, the emerging liquid phase is still weakly subdiffusive (although with a clearly faster MSD, if compared to the companion glass). This can be attributed to a liquid structure that is still in development as the glass shrinks in size. In Figure 4 (c), the system with only liquid phase shows already a normal diffusion scenario. By contrast, Figure 5 (a), at higher packing fraction ( $\phi = 0.55$ ), shows a single crystal configuration, with the diffusive part of the MSD close to stagnation (zero time growth of the MSD); i.e., the dynamics is very strongly subdiffusive, as an evidence of crystalline diffusion [29]. In the case of crystal-liquid coexistence, Figure 5 (b), the less disordered phase (glass) clearly undergoes subdiffusion, whereas the liquid has normal diffusion. Normal diffusion can also be seen in Figure 5 (c), where the single liquid phase is recovered. As we said before, and is still worth to remark here again, an important and surprising result is the confirmation, in view of the MSD behavior illustrated in Figure 4, of a glassy transitions with clear caging processes at low densities, when in general these processes are observed (to the best of our knowledge) in dense granular fluids [72]. This result may be the outcome of an effective potential developed by the interaction between the spherical balls through the intermediate air flow. In the same way, the crystal appears at unusually low densities, in comparison with the case of hard particles [44].



### 3.2. Diffusion coefficient

From the results in Figures 4, 5, we may conclude that the evolution of the MSD for each phase is qualitatively very different, which confirms our identification of the different observed phases, as previously discussed. Next, we compute the diffusion coefficient separately for each phase in this section. We represent in two figures our measurements of the diffusion coefficient. In Figure 6,  $D$  is represented vs. packing fraction, for a series of experiments in different ranges of  $T$ :  $T/m < 0.6 \sigma^2/s^2$ ;  $0.6 \sigma^2/s^2 < T/m < 0.8 \sigma^2/s^2$ ;  $0.8 \sigma^2/s^2 < T/m < 1.2 \sigma^2/s^2$  and  $T/m > 1.2 \sigma^2/s^2$ , whereas in Figure 7, we plot  $D$  vs.  $T$  for three representative packing fraction values ( $\phi = 0.18; 0.46; 0.55$ ).

Figure 6 highlights the diffusive stages of the different phase configurations, including those with phase coexistence (the coexisting phases are here joined with dashed vertical lines). As we can see, at  $T/m < 0.6 \sigma^2/s^2$  (top left panel), the diffusion coefficient tends in general to decrease for increasing  $\phi$ . Moreover, only glass or liquid phases are visible at very low  $T$ , with the liquid coexisting with the glass at low packing fractions whereas at intermediate packing fractions we find crystal-liquid coexistence and at larger  $\phi$  only the crystal is detected, in this case with the lowest  $D$  values. At higher intermediate temperatures (at  $0.6 \sigma^2/s^2 < T/m < 0.8 \sigma^2/s^2$ , in top right panel; and at  $0.8 \sigma^2/s^2 < T/m < 1.2 \sigma^2/s^2$ , bottom left) we can see the glass-liquid at low density again the effects of larger  $T$  cause the withdrawal of the crystal-liquid coexistence at intermediate  $\phi$ , leaving the liquid (red symbols) alone. Again, at higher  $\phi$ , crystal-liquid and crystal are detected. Finally, in the largest range of values of  $T$ , it is apparent that only the liquid is observed (except for a configuration with the densest system we used) and that in this regime the diffusion coefficient is nearly constant with respect to packing fraction, except for a steep decay at large  $\phi$  (where the only two cases of coexistence with a crystal are here observed). It is also interesting to note that an extrapolation of the curve averaged by the crystalline states extends to the low-density glass transition zones. In summary,  $D$  tends to decrease for denser systems, except at very high  $T$ , where it tends to keep approximately constant.

Now, in Figure 7, which represents  $D$  vs.  $T$ , summarizes well the quantitative differences in the diffusion coefficient for the three phases (glass, liquid, crystal), together with the ranges of coexistence of glass and crystal with the liquid phase. Overall, liquid predominates at low and moderate density (left and center panels), whereas glass and crystal predominate at very low and high density respectively. It can also be observed that both glass and crystal are less diffusive than the liquid, as it was to be expected, with the crystal having the lowest values, systematically, of the diffusion coefficient.

It is important to remark here that Figures 6, 7 are plenty with evidences of finite differences of the diffusion coefficient in the same system state, as a strong experimental proof of discontinuous phase transition and phase coexistence. Moreover, we have not observed in any case a continuously changing diffusion coefficient between the different phases.

As we mentioned before, previously to computing the diffusion coefficient we determine the diffusive exponent  $\alpha$  as defined by eq. (2), and whose value defines if the system is under super-diffusion ( $\alpha > 1$ ), sub-diffusion ( $\alpha < 1$ ) or normal diffusion ( $\alpha = 1$ ) [71,73]. So, we plot in Figure 8 the measurement of  $\alpha$  for all the performed experiments altogether. They are represented as a function system granular temperature  $T$  for all the particle densities combined (here, represented in the form of packing fraction  $\phi$ ). Red points signal the liquid phase diffusive exponents, green stands for the glass phase and blue for the crystal. Note the logical order of  $\alpha$  by phases, with the crystal having the lowest values, the glass in the intermediate region and the liquid having the largest  $\alpha$ . Also, as we can see, the crystal and also glass phases are very subdiffusive. The liquid however can be either weakly sub-diffusive or weakly superdiffusive. Superdiffusive values ( $\alpha > 1$ ) are reached after phase coexistence has vanished; i.e., the pure liquid phase tends to be superdiffusive, which we think is an indication again of repulsive forces between the particles. Specially at not large densities, repulsion between particles may aide the particles diffuse in between neighboring particles, thus enhancing diffusion.

### 3.3. Velocity autocorrelations

We also represented the velocity autocorrelation function, computing its trend for glass, liquid and crystal. Velocity autocorrelations provide information on the dynamics of particle collision, in particular on the statistical relation between pre-collisional and post-collisional velocities. We define the velocity autocorrelation function at lag time  $\tau$  as usual [17]

$$A_v(\tau) = \frac{\langle \mathbf{v}(t) \cdot \mathbf{v}(t + \tau) \rangle}{\langle \mathbf{v}(t) \cdot \mathbf{v}(t) \rangle}, \quad (3)$$

where here  $\langle \dots \rangle$  stands for ensemble averaging over all steady states at initial times  $t_0$ . Figure 9 represents velocity correlations  $A_v(\tau)$  in the glass-liquid transition and Figure 10 represents  $A_v(\tau)$  for the crystal-liquid transition. It is

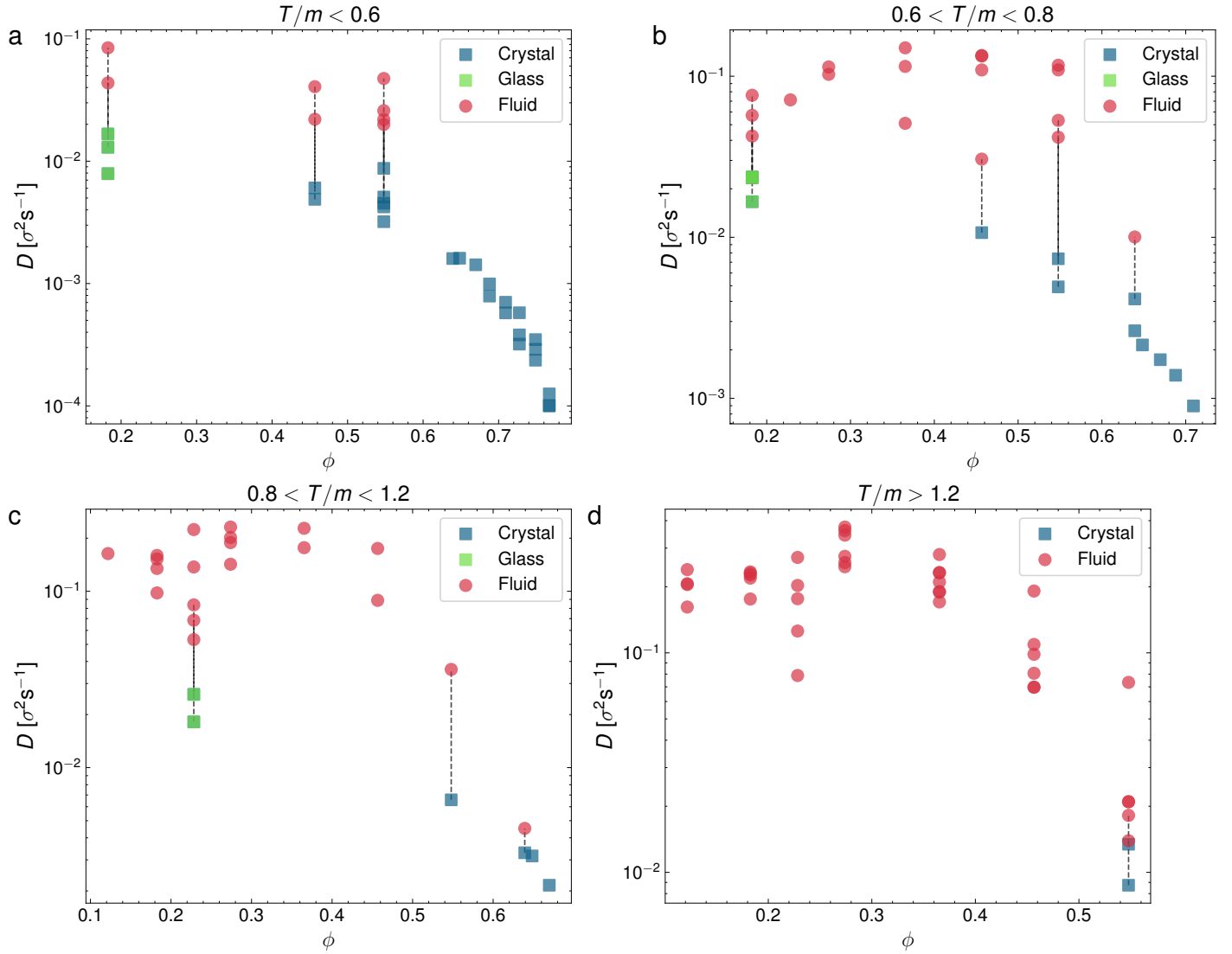


**Figure 6.** Diffusion coefficient  $D$  vs. packing fraction  $\phi$  divided in four panels by the overall granular temperature of each experiment.

to be noted that particles in the glass phase (left panel in Figure 9) show strong velocity anticorrelations at early times ( $A_v(\tau < 1) < 0$ ) and that these anticorrelations are transmitted to the coexisting liquid (center panel of Figure 9). Surprisingly as well, the depth of the anticorrelation well is increased in the glass-liquid two-phase system, with respect to the pure glass (left panel). Furthermore, the liquid remains anticorrelated at  $\tau < 1$  even when the glass has disappeared at high  $T$ . By contrast, the pure liquid phase does not display autocorrelations in the crystal-liquid transition (right panel in Figure 10), as well as an increase in the time required for the autocorrelation function to cancel for the first time. However, there are weaker anticorrelations in the pure crystal (left panel in Figure 10) and crystal-liquid two-phase state, and a very short time for the first cancellation of the autocorrelation function, typical of the crystal phase. Let us remark here that the right panels in Figures 9, 10 combined reveal that the liquid phase has a variety of internal behaviors. This variety of behavior is closely related to the occurrence of the glass transition at low densities, because as mentioned before, at low densities there is a repulsive interaction between the particles mediated by the upward air flow (as if they had a soft core with a diameter greater than that of the balls), and when the density is increased, this effective potential does not prevent the direct collision between the spherical balls.

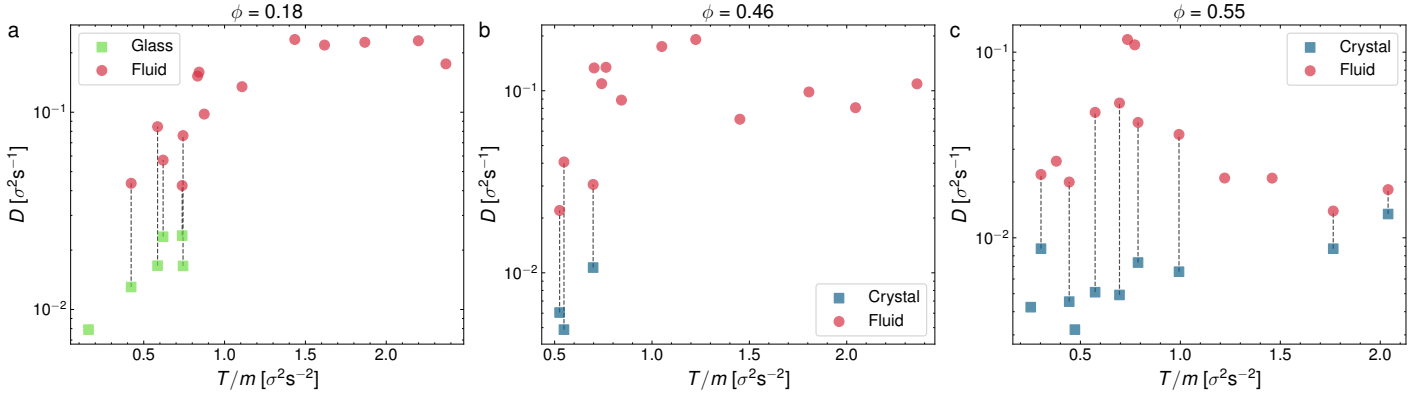


**Figure 7.** Average diffusion coefficients represented against granular temperature for three different packing fractions. Each point corresponds to an experiment; where coexistence is visible, we have split  $D$  into two different points, for the fluid (red) and crystal/glass phase (blue/green).

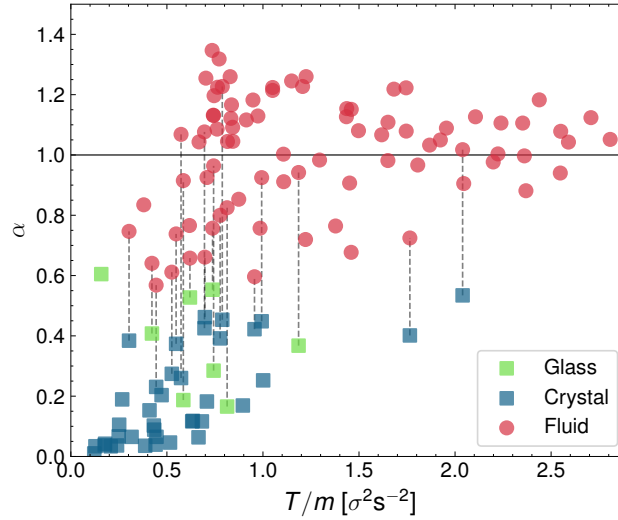


**Figure 8.** Diffusive exponent represented against granular temperature for all experiments. It has been calculated by averaging the logarithmic slope of the MSD in the [3-6] s range. Each point corresponds to an experiment; where coexistence is visible, we have split  $D$  into two different points, for the fluid (red) and crystal/glass phase (blue/green).

#### 4. Discussion

We have studied the nearly-2D dynamics of a system of rolling (inelastic) spheres. The dynamics of the set of spheres is activated by means of the turbulent vortices that originate out of an air upflow past the spheres. As we have seen, the phase behavior of the system is very complex, and we have been able to detect an arrest phase (particles that remain still or static for low energy input), a glass phase (disordered lattice of Brownian particles with sporadic jumps to other lattice positions), a liquid (completely disordered phase) and a hexagonal crystal. In particular, the glass phase appears at very low densities, which to our knowledge is a very rare situation [70]. This undoubtedly is due to long-ranged repulsive forces between the air-fluidized particles that have been reported previously [54]. However, this kind of low density granular glass had not been reported previously, to the best of our knowledge. Moreover, the glass and the hexagonal crystal can coexist with the liquid (again, glass-liquid coexistence had not been reported previously in the context of granular dynamics, to the best of our knowledge). Additionally, the glass can also coexist with the arrest phase, at low air current (dynamics in the process of activation, again not detected previously). In fact, the dynamics of the system is so complex that we have been able to detect important qualitative differences in the behavior of a single phase. For instance, as we mentioned above, the velocities of particles in the liquid phase can be either strongly anticorrelated at early times

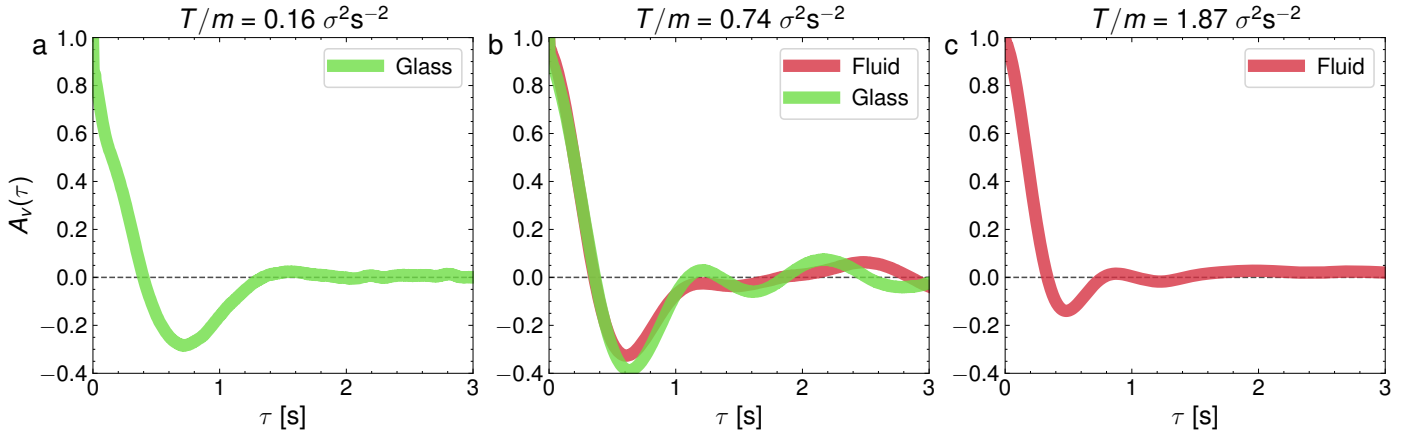


**Figure 9.** Normalized velocity autocorrelation for three different temperatures at  $\phi = 0.18$ . They correspond to the cases presented for the MSD in Figure 4.

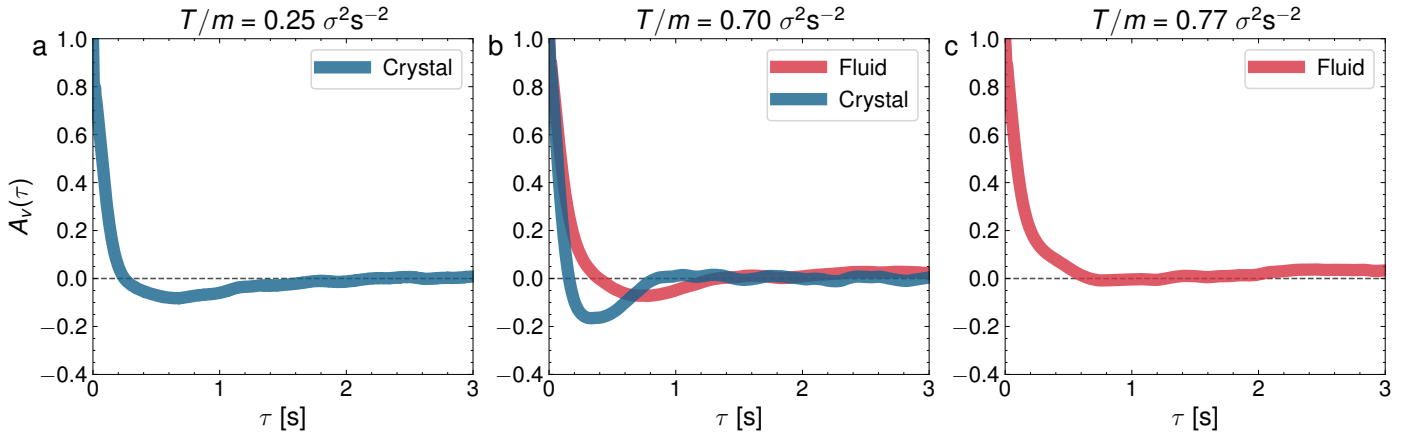


**Figure 10.** Normalized velocity autocorrelation for three representative experiments of  $\phi = 0.55$ . They correspond to the cases presented for the MSD in Figure 5.

or not anticorrelated at all, depending on the configuration of the system. As another example, the crystal can display vanishing diffusive exponent (and in any case, the crystal is always strongly subdiffusive, see Figure 8).

In general, the diffusive properties of the observed phases are rather different. Both the glass and the crystal are always subdiffusive, and present anticorrelated velocities. By contrast, the liquid presents always nearly normal diffusion (departures from normal diffusion can be attributed here either to measurement error or to limitations of our set-up). Measurement of the granular temperature field confirms that in all cases of phase coexistence there is a significant energy non-equipartition. This enhances the idea that these transitions are occurring in states very far from equilibrium. It may be that because of this (that our experimental configurations seem to be very far away from equilibrium) that the phase transition scenario here described completely differs from the KTHNY scenario described for 2D equilibrium systems [43] and also, under certain conditions, in non-equilibrium systems such as a vibrated granular monolayer [44,45] and 2D active brownian disks [53]. Here, however, this KTHNY scenario is as we said absent and the hexatic phase has not been observed in any situation, which is a very peculiar situation in the context of two-dimensional matter. Furthermore, all transitions we observed in this work occur through phase coexistence, contrary to the scenario of liquid-hexatic-crystal continuous phase transition without coexistence described in the KTHNY theory. Specifically, the fact that the hexagonal crystal in our set-up melts by shrinking in size, giving rise a growing liquid and the transition is not defect-mediated, guarantees the complete absence of a hexatic phase during the melting process. Therefore, our results differ fundamentally in this aspect from previous results in both equilibrium and non-equilibrium systems (where the hexatic phase has always

been observed, at least, under certain conditions). It remains for future work to study in more detail the structure of this intriguing phase behavior.

**Author Contributions:** J.F. G.-S. and M. A. L.-C. performed all the experiments. M. A. L.-C. and F. V. R. developed the particle tracking and processing codes. M.A. L.-C. prepared all figures. All authors participated in the formal analysis of the experimental data. A. R.-R. and F. V. R. reviewed and edited the manuscript. Design of the experiment, conceptualization, original draft preparation, and supervision was performed by F. V. R. All authors have read and agreed to the published version of the manuscript.

**Funding:** We acknowledge funding from the Government of Spain through Agencia Estatal de Investigación (AEI) project No. PID2020-116567GB-C22). A.R.-R. also acknowledges financial support from Consejería de Transformación Económica, Industria, Conocimiento y Universidades de la Junta de Andalucía/FEDER for funding through project P20-00816 and FSE through post-doctoral grant no. DC00316 (PAIDI 20201). F. V. R. is supported by the Junta de Extremadura grant No. GR21091, partially funded by the ERDF. The APC was funded by the MDPI editorial.

**Data Availability Statement:** Experimental data tables and trajectories are available in a public repository, at: <https://doi.org/10.5281/zenodo.7097642>.

**Acknowledgments:** The authors are indebted to the Taller de Mecánica de la Escuela de Ingenierías Industriales for construction contributions to the design of the air table. The authors are also thankful to Prof. S. B. Yuste and E. Abad for their important contributions to error measurement in the early stages of this project.

**Conflicts of Interest:** The authors declare no conflict of interest.

## References

1. Jaeger, H.M.; Nagel, S.; Behringer, R. The physics of granular materials. *Physics Today* **1996**, *49*, 32.
2. de Gennes, P.G. Granular matter: a tentative view. *Rev. Mod. Phys.* **1999**, *71*, S374–S382.
3. Aranson, I.S.; Tsimring, L.S. Patterns and collective behavior in granular media: Theoretical concepts. *Rev. Mod. Phys.* **2006**, *78*, 641–692. <https://doi.org/10.1103/RevModPhys.78.641>.
4. Olafsen, J.S.; Urbach, J.S. Clustering, order and collapse in a driven granular monolayer. *Phys. Rev. Lett* **1998**, *81*, 4369–4372.
5. Goldhirsch, I. Rapid Granular Flows. *Annu. Rev. Fluid Mech.* **2003**, *35*, 267–293.
6. Vega Reyes, F.; Urbach, J.S. Steady base states for Navier-Stokes granular hydrodynamics with boundary heating and shear. *J. Fluid Mech.* **2009**, *636*, 279.
7. Gantzounis, G.; Yang, J.; Kevrekidis, P.G.; Daraio, C. Granular acoustic switches and logic elements. *Nat. Commun.* **2014**, *5*, 5311. <https://doi.org/10.1038/ncomms6311>.
8. González-Saavedra, J.F.; Rodríguez-Rivas, Á.; López-Castaño, M.A.; Vega Reyes, F. Acoustic Resonances in a Confined Set of Disks. In Proceedings of the Traffic and Granular Flow 2019; Zuriguel, I.; Garcimartin, A.; Cruz, R., Eds.; Springer International Publishing: Cham, 2020; pp. 349–355.
9. Mujica, N.; Soto, R. Dynamics of noncohesive confined granular media. *Environmental Science and Engineering (Subseries: Environmental Science)* **2016**, pp. 445–463.
10. Zik, O.; Stavans, J. Self-Diffusion in Granular Flows. *Europhysics Letters (EPL)* **1991**, *16*, 255–258. <https://doi.org/10.1209/0295-5075/16/3/006>.
11. Oger, L.; Annic, C.; Bideau, D.; Dai, R.; Savage, S.B. Diffusion of two-dimensional particles on an air table. *J. Stat. Phys.* **1996**, *82*, 1047.
12. Ojha, R.P.; Lemieux, P.A.; Dixon, P.K.; Liu, A.J.; Durian, D.J. Statistical mechanics of a gas-fluidized particle. *Nature* **2004**, *427*, 521.
13. Rosato, A.; Strandburg, K.J.; Prinz, F.; Swendsen, R.H. Why the Brazil nuts are on top: Size segregation of particulate matter by shaking. *Phys. Rev. Lett.* **1987**, *58*, 1038–1040. <https://doi.org/10.1103/PhysRevLett.58.1038>.
14. Kondic, L.; Hartley, R.R.; Tennakoon, S.G.K.; Painter, B.; Behringer, R.P. Segregation by friction. *EPL* **2003**, *61*, 742.
15. Jenkins, J.T.; Yoon, D.K. Segregation in Binary Mixtures under Gravity. *Phys. Rev. Lett.* **2002**, *88*, 194301. <https://doi.org/10.1103/PhysRevLett.88.194301>.
16. Hill, K.M.; Khakhar, D.V.; Gilchrist, J.F.; McCarthy, J.J.; Ottino, J.M. Segregation-driven organization in chaotic granular flows. *Proceedings of the National Academy of Sciences* **1999**, *96*, 11701–11706, [<https://www.pnas.org/doi/pdf/10.1073/pnas.96.21.11701>]. <https://doi.org/10.1073/pnas.96.21.11701>.
17. Melby, P.; Vega Reyes, F.; Prevost, A.; Robertson, R.; Kumar, P.; Egolf, D.A.; Urbach, J.S. The dynamics of thin vibrated granular layers. *J. Phys.: Condens. Matter* **2005**, *17*, S2369.
18. Eshuis, P.; van der Weele, K.; van der Meer, D.; Bos, R.; Lohse, D. Phase diagram of vertically shaken granular matter. *Phys. Fluids* **2007**, *19*, 123301.



19. McLaren, C.P.; Kovar, T.M.; Penn, A.; Müller, C.R.; Boyce, C.M. Gravitational instabilities in binary granular materials. *Proceedings of the National Academy of Sciences* **2019**, *116*, 9263–9268. <https://doi.org/10.1073/pnas.1820820116>.
20. He, X.; Meerson, B.; Doolen, G. Hydrodynamics of thermal granular convection. *Phys. Rev. E* **2002**, *65*, 030301. <https://doi.org/10.1103/PhysRevE.65.030301>.
21. Pontuale, G.; Gnoli, A.; Puglisi, A.; Vega Reyes, F. Thermal Convection in Granular Gases with Dissipative Lateral Walls. *Phys. Rev. Lett.* **2017**, *117*, 098006.
22. Isobe, M. Statistical law of turbulence in granular gas. *J. Phys. Conf. Ser.* **2012**, *402*, 012041.
23. Isobe, M. Velocity statistics in two-dimensional granular turbulence. *Phys. Rev. E* **2003**, *68*, 040301(R).
24. Liu, A.; Nagel, S. Jamming is not just cool anymore. *Nature* **1998**, *396*, 21–2.
25. Daniels, L.J.; Haxton, T.K.; Xu, N.; Liu, A.J.; Durian, D.J. Temperature-pressure scaling for air-fluidized grains near jamming. *Physical Review Letters* **2012**, *108*, 1–5, [arXiv:1110.5611v1]. <https://doi.org/10.1103/PhysRevLett.108.138001>.
26. Lasanta, A.; Vega Reyes, F.; Prados, A.; Santos, A. When the Hotter Cools More Quickly: Mpemba Effect in Granular Fluids. *Phys. Rev. Lett.* **2017**, *119*, 1–6, [1611.04948]. <https://doi.org/10.1103/PhysRevLett.119.148001>.
27. Keim, N.C.; Paulsen, J.D.; Zeravcic, Z.; Sastry, S.; Nagel, S.R. Memory formation in matter. *Rev. Mod. Phys.* **2019**, *91*, 035002. <https://doi.org/10.1103/RevModPhys.91.035002>.
28. Prevost, A.; Melby, P.; Egolf, D.A.; Urbach, J.S. Nonequilibrium two-phase coexistence in a confined granular layer. *Phys. Rev. E* **2004**, *70*, 050301. <https://doi.org/10.1103/PhysRevE.70.050301>.
29. Reis, P.M.; Ingale, R.A.; Shattuck, M. Crystallization of a quasi-two-dimensional granular fluid. *Phys. Rev. Lett.* **2006**, *96*, 258001.
30. Vega Reyes, F.; Urbach, J.S. Effect of inelasticity on the phase transitions of a thin vibrated granular layer. *Phys. Rev. E* **2008**, *78*, 051301. <https://doi.org/10.1103/PhysRevE.78.051301>.
31. Castillo, G.; Mujica, N.; Soto, R. Criticality of a Granular Solid-Liquid-Like Phase Transition. *Phys. Rev. Lett.* **2012**, *109*, 095701.
32. Néel, B.; Rondini, I.; Turzillo, A.; Mujica, N.; Soto, R. Dynamics of a first-order transition to an absorbing state. *Phys. Rev. E* **2014**, *89*, 042206. <https://doi.org/10.1103/PhysRevE.89.042206>.
33. Castillo, G.; Mujica, N.; Soto, R. Universality and criticality of a second-order granular solid-liquid-like phase transition. *Phys. Rev. E* **2015**, *91*, 012141. <https://doi.org/10.1103/PhysRevE.91.012141>.
34. Vega Reyes, F.; Santos, A.; Garzó, V. Non-Newtonian Granular Hydrodynamics. What Do the Inelastic Simple Shear Flow and the Elastic Fourier Flow Have in Common? *Phys. Rev. Lett.* **2010**, *104*, 028001. <https://doi.org/10.1103/PhysRevLett.104.028001>.
35. Rietz, F.; Radin, C.; Swinney, H.L.; Schröter, M. Nucleation in Sheared Granular Matter. *Phys. Rev. Lett.* **2018**, *120*, 055701.
36. Goldhirsch, I.; Zanetti, G. Clustering instability in dissipative gases. *Phys. Rev. Lett.* **1993**, *70*, 1619–1622.
37. Prevost, A.; Egolf, D.A.; Urbach, J.S. Forcing and Velocity Correlations in a Vibrated Granular Monolayer. *Phys. Rev. Lett.* **2002**, *89*, 084301. <https://doi.org/10.1103/PhysRevLett.89.084301>.
38. Mujica, N.; Soto, R. Dynamics of Noncohesive Confined Granular Media. In *Proceedings of the Recent Advances in Fluid Dynamics with Environmental Applications*; Klapp, J.; Sigalotti, L.D.G.; Medina, A.; López, A.; Ruiz-Chavarría, G., Eds.; Springer International Publishing: Cham, 2016; pp. 445–463.
39. Kosterlitz, J.M.; Thouless, D.J. Long range order and metastability in two dimensional solids and superfluids. (Application of dislocation theory). *J. Phys. C* **1972**, *5*, L124–L126.
40. Kosterlitz, J.M.; Thouless, D.J. Ordering, metastability and phase transitions in two-dimensional systems. *J. Phys. C* **1973**, *6*, 1181.
41. Nelson, D.R.; Halperin, B.I. Dislocation mediated melting in two dimensions. *Phys. Rev. B* **1979**, *19*, 2457.
42. Young, A.P. Melting and the vector Coulomb gas in two dimensions. *Phys. Rev. B* **1979**, *19*, 1855.
43. Strandburg, K.J. Two-dimensional melting. *Rev. Mod. Phys.* **1988**, *60*, 161.
44. Olafsen, J.S.; Urbach, J.S. Two-Dimensional Melting Far from Equilibrium in a Granular Monolayer. *Phys. Rev. Lett.* **2005**, *95*, 098002.
45. Komatsu, Y.; Tanaka, H. Roles of Energy Dissipation in a Liquid-Solid Transition of Out-of-Equilibrium Systems. *Phys. Rev. X* **2015**, *5*, 031025.
46. Foerster, S.F.; Louge, M.Y.; Chang, H.; Allia, K. Measurements of the collision properties of small spheres. *Physics of Fluids* **1994**, *6*, 1108–1115, [https://doi.org/10.1063/1.868282]. <https://doi.org/10.1063/1.868282>.
47. Foerster, S.F.; Louge, M.Y.; Chang, H.; Allia, K. Measurements of the collision properties of small spheres. Experimental data table. Technical report, 1994.
48. Olafsen, J.S.; Urbach, J.S. Velocity distributions and density fluctuations in a granular gas. *Phys. Rev. E* **1999**, *60*, R2468.
49. Olafsen, J.S.; Urbach, J.S., Experimental observations of non-equilibrium distributions and transitions in a 2D granular gas; Springer-Verlag: Berlin, Germany, 2001; Vol. Granular Gases, *Lecture Notes in Physics*, pp. 410–428.
50. Brey, J.J.; Dufty, J.W.; Kim, C.S.; Santos, A. Hydrodynamics for granular flow at low density. *Physical Review E* **1998**, *58*, 4638–4653. <https://doi.org/10.1103/PhysRevE.58.4638>.
51. Brey, J.J.; Cubero, D., Hydrodynamic transport coefficients of granular gases; Springer-Verlag: Berlin, Germany, 2001; Vol. Granular Gases, *Lecture Notes in Physics*, pp. 59–78.

52. Bechinger, C.; Di Leonardo, R.; Löwen, H.; Reichhardt, C.; Volpe, G.; Volpe, G. Active particles in complex and crowded environments. *Rev. Mod. Phys.* **2016**, *88*, 045006. <https://doi.org/10.1103/RevModPhys.88.045006>.
53. Digregorio, P.; Levis, D.; Suma, A.; Cugliandolo, L.F.; Gonnella, G.; Pagonabarraga, I. Full Phase Diagram of Active Brownian Disks: From Melting to Motility-Induced Phase Separation. *Phys. Rev. Lett.* **2018**, *121*, 098003. <https://doi.org/10.1103/PhysRevLett.121.098003>.
54. Ojha, R.P.; Abate, A.R.; Durian, D.J. Statistical characterization of the forces on spheres in an upflow of air. *Phys. Rev. E* **2005**, *71*, 016313. <https://doi.org/10.1103/PhysRevE.71.016313>.
55. Batchelor, G.K. Transport properties of two-phase materials with random structure. *Ann. Rev. Fluid Mech.* **1974**, *6*, 227–255.
56. Ojha, R.P.; Abate, A.R.; Durian, D.J. Statistical characterization of the forces on spheres in an upflow of air. *Phys. Rev. E* **2005**, *71*, 016313.
57. López-Castaño, M.A.; González-Saavedra, J.F.; Rodríguez-Rivas, A.; Abad, E.; Yuste, S.B.; Vega Reyes, F. Pseudo-two-dimensional dynamics in a system of macroscopic rolling spheres. *Phys. Rev. E* **2021**, *103*, 042903. <https://doi.org/10.1103/PhysRevE.103.042903>.
58. Abate, A.R.; Durian, D.J. Partition of energy for air-fluidized grains. *Phys. Rev. E* **2005**, *72*, 031305.
59. López-Castaño, M.A.; González-Saavedra, J.F.; Rodríguez-Rivas, A.; Vega Reyes, F. Statistical Properties of a Granular Gas Fluidized by Turbulent Air Wakes. In Proceedings of the Traffic and Granular Flow 2019; Zuriguel, I.; Garcimartin, A.; Cruz, R., Eds.; Springer International Publishing: Cham, 2020; pp. 397–403.
60. Koyama, S.; Matsuno, T.; Noguchi, T. Anomalous diffusion in a monolayer of lightweight spheres fluidized in air flow. *Phys. Rev. E* **2021**, *104*, 054901. <https://doi.org/10.1103/PhysRevE.104.054901>.
61. Maw, N.; Barber, J.R.; Fawcett, J.N. The Role of Elastic Tangential Compliance in Oblique Impact. *Journal of Lubrication Technology* **1981**, *103*, 74–80, [[https://asmedigitalcollection.asme.org/tribology/article-pdf/103/1/74/5796519/74\\_1.pdf](https://asmedigitalcollection.asme.org/tribology/article-pdf/103/1/74/5796519/74_1.pdf)]. <https://doi.org/10.1115/1.3251617>.
62. Taneda, S. Visual observations of the flow past a sphere at Reynolds numbers between  $10^4$  and  $10^6$ . *J. Fluid Mech.* **1978**, *85*, 187–192.
63. Van Dyke, M. *An album of fluid motion*; The Parabolic Press: Stanford, CA, USA, 1982.
64. Montanero, J.M.; Garzó, V.; Santos, A.; Brey, J.J. Kinetic theory of simple granular shear flows of smooth hard spheres. *J. Fluid Mech.* **1999**, *389*, 391–411.
65. OpenCV. <https://opencv.org/>.
66. Allan, D. *et al.*. soft-matter/trackpy: Trackpy v0.4.2, 2019.
67. Vega Reyes, F.; López-Castaño, M.A.; Rodríguez-Rivas, A., 2022.
68. Kanatani, K.I. A micropolar continuum theory for the flow of granular materials. *Int. J. Engng. Sci.* **1979**, *17*, 419–432.
69. Desmond, K.W.; Weeks, E.R. Random close packing of disks and spheres in confined geometries. *Physical Review E - Statistical, Nonlinear, and Soft Matter Physics* **2009**, *80*, 1–11, [0903.0864]. <https://doi.org/10.1103/PhysRevE.80.051305>.
70. Rodríguez-Rivas, A.; Romero-Enrique, J.M.; Rull, L.F. Molecular simulation study of the glass transition in a soft primitive model for ionic liquids. *Mol. Phys.* **2019**, *117*, 3941–3956. <https://doi.org/10.1080/00268976.2019.1674935>.
71. Metzler, R.; Jeon, J.H.; Cherstvy, A.G.; Barkai, E. Anomalous diffusion models and their properties: non-stationarity, non-ergodicity, and ageing at the centenary of single particle tracking. *Phys. Chem. Chem. Phys.* **2014**, *16*, 24128–24164. <https://doi.org/10.1039/C4CP03465A>.
72. Kranz, W.T.; M. Sperl,.; Zippelius, A. Glass Transition for Driven Granular Fluids. *Phys. Rev. Lett.* **2010**, *104*.
73. López-Castaño, M.A.; Vega Reyes, F.; Rodríguez-Rivas, A. Diffusive regimes in a two-dimensional chiral fluid. *Comms. Phys.* **2022**, to appear. preprint: arXiv:2202.08920.